ISSN 0915-633X

NATIONAL INSTITUTE FOR FUSION SCIENCE

Catastrophes with Indeterminate Outcome

H. B. Stewart and Y. Ueda

(Received – Sep. 20, 1990)

NIFS-56 Oct. 1990

RESEARCH REPORT
NIFS Series

NAGOYA, JAPAN

Submitted to Proc. R. Soc. Lond. A.

Catastrophes with indeterminate outcome*

H. B. STEWART

Mathematical Sciences Group
Department of Applied Science
Brookhaven National Laboratory
Upton, NY 11973

and

Y. UEDA

Department of Electrical Engineering
Kyoto University
Kyoto 606, Japan

A catastrophe in a dissipative dynamical system which causes an attractor to completely lose stability will result in a transient trajectory making a rapid jump in phase space to some other attractor. In systems where more than one other attractor is available, the attractor chosen may depend very sensitively on how the catastrophe is realized. Two examples in forced oscillators of Duffing type illustrate how the probabilities of different outcomes can be estimated using the phase space geometry of invariant manifolds.

*This work was supported by the Applied Mathematical Sciences program of the U.S. Department of Energy under Contract No. DE-AC02-76CH00016.

In attempting to understand the bifurcation behavior of a dissipative dynamical system, the applied dynamicist will naturally focus attention first on those bifurcations which are catastrophic in the sense that an attractor, a basin boundary, or some other invariant set in phase space undergoes a discontinuous change (Zeeman 1982). Catastrophic bifurcations manifest themselves clearly in common experimental scenarios. For example, a dynamical system may be allowed to evolve over a long time, so that its behavior settles to an attractor; a small step change $\Delta\mu$ is made to a control parameter μ, and the system is again allowed to settle, often to the same attractor with only small quantitative changes. After several further small increments from μ_i to $\mu_{i+1} = \mu_i + \Delta\mu$, a threshold value μ_I may be reached across which the attractor changes its quantitative description by an unexpectedly large amount which appears, by comparison with previous incremental steps, to be out of all proportion to the small size of $\Delta\mu$. This result is evidence that a catastrophic bifurcation has occurred at some value of μ between μ_I and μ_{I+1}. Another common scenario for observing attractor bifurcations is to ramp the control μ very slowly, so in the interval of time ΔT needed to identify and characterize an attractor, the corresponding change $\Delta\mu$ has usually (except crossing catastrophic thresholds) only a small quantitative effect on the attractor.

The most severe catastrophic bifurcation is the total loss of stability of an attractor, so that when μ is stepped from μ_I to μ_{I+1}, the system experiences a transient jump followed by settling to another attractor, whose location in phase space is remote from the attractor sustained at $\mu = \mu_I$. This sudden disappearance of an attractor from the phase portrait is a blue sky catastrophe (Abraham 1985), or boundary crisis

(Grebogi et al. 1983).

Suppose the dynamical system can be reset to control $\mu = \mu_I$ and to state values such that the old attractor is re-established. Then it may happen that a second experimental trial stepping from μ_I to μ_{I+1} causes the system to jump to some new attractor different from the outcome of the previous trial. In fact, the system is extremely sensitive to details of how the bifurcation is realized experimentally, such as the exact size of $\Delta\mu$, or the precise rate at which μ is ramped.

Recently Abraham (1985) suggested a geometric control-phase space model for this behavior using a codimension two bifurcation scenario of Andronov and Takens (1974). Abraham's model involves a dynamical system represented by a flow in planar phase space with one periodic attractor surrounding two static point attractors, and having two generic control parameters which follow a circular path in control space around a codimension two point. At one point along this path, a dynamic saddle-node fold bifurcation removes the periodic attractor. The basin structure of the remaining two point attractors is intertwined so that the outcome of evolving a system slowly through the bifurcation would depend very sensitively on the speed with which the controls are ramped. Equivalently, the outcome of a small step increment of the controls across the bifurcation threshold would depend very sensitively on the precise size of the increment. The global geometry of this bifurcation scenario is illustrated in Figure 8 of Abraham (1985) and in Figure 69 of Abraham and Shaw (1987).

Our purpose here is to note that a simple generalization of this geometric model to a planar diffeomorphism can be observed in the Duffing oscillator. This example involves transverse heteroclinic inter-

sections of invariant manifolds, but no homoclinic intersections. We also give a second example in the twin-well Duffing oscillator involving additional homoclinic structures: the vanishing attractor is chaotic, in fact a simply folded band (Rössler 1975); and the remaining two basins have a common boundary which is fractal. In each example, we show how the probabilities of the two outcomes can be roughly estimated from the coordinates of a few heteroclinic points. However, in the second example, the fractal basin structure implies outcome uncertainty of a qualitatively different and more severe type, and greater obstacles to obtaining better than a crude estimate of outcome probabilities. Our examples are closely related to the observation by Thompson and Soliman (1990) of a fold bifurcation leading to indeterminate jumps to competing attractors with fractal basin boundaries.

Our first example occurs in Duffing's equation

$$\ddot{x} + k\dot{x} + x^3 = B\cos t \tag{1}$$

with $k = 0.05$ and $B = 0.0574$. Figure 1 shows the basins of three competing periodic attractors in Poincaré section at angle $t = 0$ of the cosinusoidal forcing. This and subsequent portraits were computed with a fourth-order Runge-Kutta integration formula using fixed time steps of $2\pi/60$. Two of the attractors are fixed points, marked by small circles: ${}^1S$ near the top of Figure 1a, and ${}^2S$ near the center of Figure 1a. Also present is a subharmonic attractor of order 3, i.e. of period 6π, whose three image points are marked by the small filled triangles in the interiors of the three white regions. The shading of Figure 1 was determined by exhaustively integrating initial conditions on a 201×201 point grid until final behavior was reached; an initial point was then colored grey if it settled to ${}^1S$, black if it settled to ${}^2S$,

or left white if it settled to the period 3 attractor, which we denote by S^3. This phase portrait is similar to Figure 10.6 of Hayashi (1964), with $k = 0.1$ and $B = 0.15$, and is close to the (a) regime in the (k, B) survey of Ueda (1980); but here we have adjusted k and B to bring the attracting fixed point ${}^1S$ close to a fold bifurcation involving saddle D, whose inset or stable manifold defines the boundary of the basin of ${}^1S$.

We use the notation ${}^{\mathrm{i}}S^{\mathrm{j}}_{\mathrm{k}}$ for periodic points, where the index j is the period (if greater than one), i distinguishes different orbits of the same period (if more than one are present), and $\mathrm{k} = 1, 2, \ldots \mathrm{j}$ identifies successive images of a periodic orbit under iteration of the Poincaré map. Thus ${}^1S$ and ${}^2S$ are two distinct fixed points; because each has period one, the indices j and k are suppressed. On the other hand, S^3 is the only stable periodic orbit with period 3, and so the index i is suppressed; if the three points of this orbit were to be distinguished, we should label them S^3_1, S^3_2, and S^3_3.

The common boundary of the basins of ${}^2S$ and S^3 is defined by the inset or stable manifold of a period 3 saddle D^3 marked by small hollow triangles, as illustrated in Figure 2. The tails of these two basins wind around ${}^2S$ and S^3 repeatedly, becoming infinitely thin as they accumulate along the basin boundary of ${}^1S$. This accumulation is seen in the detailed portrait Figure 1b, and can be inferred from the existence of heteroclinic points lying in both the outset or stable manifold of D (indicated by the dashed curve in Figure 2) and the inset or stable manifold of D^3 (solid curves). For example, the heteroclinic point numbered 1 has as its image the point 5. Since both manifolds are invariant, all the pre-images of point 1 are also heteroclinic points,

and these pre-images accumulate at D.

As noted previously, the system at $k = 0.05$ and $B = 0.0574$ is very close to a saddle-node bifurcation. Consider the effect of disturbing this incipiently unstable system from an orbit settled on the marginally stable attractor ${}^1S$. A disturbance might be a small step increment of the parameter B to a value beyond the saddle-node disappearance of ${}^1S$ at $B \simeq 0.05738$; for simplicity, we consider instead a disturbance of the phase space coordinates which displaces the orbit at $t = 0$ from ${}^1S$ to a point below the inset of D and into the intermingled basins of ${}^2S$ and S^3, while keeping the system parameters fixed at $k = 0.05$ and $B = 0.0574$. Following such a disturbance, a transient takes the system eventually to either ${}^2S$ or S^3; and if the disturbance be just barely enough to move the system below the inset of D, to the region of most finely intermingled basins, then the attractor eventually chosen will depend very sensitively on the size of the disturbance.

Under repeated trials, with disturbances uniformly distributed transverse to and below the inset of D, well-defined probabilities may be assigned to the two outcomes ${}^2S$ and S^3. If these disturbances always put the system near D, so that a local linear approximation of the dynamics is admissible, then the probabilities can be determined from the spacing of heteroclinic points in any fundamental neighborhood of the outset of D defined by two heteroclinic points, H and its image H^* under one iteration of the Poincaré map. From Figure 2 we infer that there will be three additional heteroclinic points between any such H and H^*; the proportions of the two basins between H and H^* will be the same for segment HH^* as for all its forward and backward images near D, since each iteration forward expands segment HH^*

by λ, the expanding eigenvalue of the saddle D. Therefore any range of disturbance sizes which includes several images of this fundamental neighborhood will be divided in approximately the same proportions as HH^* itself.

To illustrate, we take the heteroclinic points 1 through 8 in Figure 2. Table 1 gives the coordinates of the eight heteroclinic points and the distances between them. Using points 1 through 5 gives an estimate of 91% ${}^2S$ outcomes and 9% S^3 outcomes; using points 4 through 8 gives 92% and 8%. A numerical experiment starting 200 orbits evenly spaced along a small interval of the outset of D very near to and below D gave 22 orbits settling to S^3 and the remaining 178 to ${}^2S$. Thus the probabilities estimated from heteroclinic points are roughly correct, with the points closer to D giving a slightly better estimate. For reference, the grid points in each basin were counted in Figure 1b, giving 12397 points in the basin of ${}^1S$, 3328 points in the basin of the period 3 attractor S^3, and 24676 points in the basin of ${}^2S$. Thus the probability of S^3outcome is $3328/(3328+24676) \simeq 12\%$.

The heteroclinic points in this example were chosen in a region of phase space where the basin structure is relatively coarse and clearly distinguishable. It is easy to imagine applications in which the finer basin structure near D would be very difficult to determine experimentally. On the other hand, in more general systems heteroclinic points far from the incipient saddle-node might give poor estimates of the outcome probabilities and heteroclinic points nearer to the saddle-node would be preferred if available.

Our second example occurs in the symmetric twin-well Duffing os-

cillator

$$\ddot{x} + k\dot{x} - x + x^3 = A\sin\omega t \tag{2}$$

derived from a quartic potential $V(x) = x^2/2 - x^4/4$ having two wells with minima at $x = \pm 1$ separated by a smooth potential barrier with maximum at $x = 0$. Under weak forcing there are two stable solutions, a periodic orbit encircling each potential minimum. Under increased forcing amplitude A, with ω less than the natural frequency $\omega_0 = \sqrt{2}$ for small undamped, unforced oscillations, the softening effect of the smooth potential barrier causes a familiar nonlinear resonance, resulting in a second coexisting attractor in each well. The response amplitude of this second periodic motion measured from the potential minimum is larger than that of the original attractor; the larger amplitude motion will be called the resonant motion.

The region in (ω, A) control space where this occurs for equation (2) with damping $k = 0.25$ is shown in Figure 3. The resonant periodic attractor is created upon crossing the fold bifurcation arc f while increasing the forcing amplitude A. Further increasing A will cause a jump to resonance if, for example, the fold arc F is crossed between the cusp point P and point S in Figure 3; the motion does not escape from its potential well, but is recaptured by the resonant attractor in the same well.

The remaining pattern of bifurcation arcs has been elucidated by Thompson (1989) in his study of conditions leading to escape from confinement within a potential well in an oscillator of Duffing type with a single, asymmetric potential well. For example, the resonant periodic attractor doubles it period as the flip bifurcation arc (broken curve) is crossed, and further period doublings lead to a chaotic at-

tractor as the bifurcation arc G is approached. Upon crossing G to the left of R (i.e. for $\omega \lesssim 1.02$) the chaotic attractor undergoes a chaotic blue sky catastrophe, and the ensuing transient is always recaptured in the same well by the coexisting nonresonant periodic attractor. This is the chaotic saddle catastrophe described by Stewart (1988). On the other hand, crossing G by increasing the forcing amplitude A to the right of Q, there is no coexisting attractor in the same well, and so the one-well chaotic attractor explodes to a large chaotic attractor whose orbits visit both potential wells. In other words, orbits escape confinement to a single well.

Here we are particularly interested in the bifurcation behavior crossing G in the broken segment between R and Q, seen more clearly in Figure 3b. Corresponding phase portraits are shown as Poincaré sections at angle $t = 0$ in Figure 4. For Figure 4a and 4b, the parameter values $\omega = 1.069, A = 0.2110$ were chosen near the maximum A value for which two attractors coexist in each well. To the right of the hilltop saddle ${}^1D$ (empty circle near the origin $x = y = 0$) are the nonresonant attracting fixed point ${}^1S$ very near the saddle ${}^2D$ in its basin boundary, and a chaotic attractor containing the inversely unstable fixed point ${}^2I$ left behind when the resonant fixed point ${}^2S$ doubled its period at $A \simeq 0.194$. To the left of ${}^1D$ are the corresponding attractors and fixed points of the left potential well. The basins of the four attractors are indicated by exhaustively solving equation (2) numerically for all initial conditions on a 201×201 grid and marking each point according to the results: no dot for a point in the basin of ${}^1S$; light grey dot for the basin of ${}^1S'$ in the left well; medium grey dot for the basin of the right well chaotic attractor; and dark grey dot for

the basin of the left well chaotic attractor. In Figure 4b, the chaotic attractor is seen to be very close to its basin boundary, which includes a period three saddle D^3 indicated by three small triangles. The blue sky catastrophe is a boundary crisis (Grebogi et al. 1983) at which the chaotic attractor touches the unstable periodic orbit D^3; indeed a very similar event has been described for the Henon map by Grebogi et al (1987). We refer to D^3 as the destroyer in this bifurcation.

Figures 4c and 4d show the corresponding phase portraits just after the chaotic blue sky catastrophe which was incipient in Figure 4b. After this bifurcation, the region formerly occupied by the basin of the chaotic attractor is now an apparently tangled mixture of the basins of ${}^1S$ and ${}^1S'$. In particular, if the system at $\omega = 1.069$ and $A = 0.2110$ with an orbit on the chaotic attractor is suddenly disturbed so that A is instantaneously stepped to 0.2116, it is clear that the outcome may be either ${}^1S$ (recapture in the same well) or ${}^1S'$ (escape to the opposite well), depending very sensitively on the initial position in the former chaotic attractor. Equivalently, if the initial position is fixed and the system experiences a disturbance ΔA which moves A across the bifurcation arc G between R and Q, the outcome will depend very sensitively on the exact size of the increment ΔA. As with our first example, we can assign well-defined probabilities to the two outcomes; clearly the probability of escape is much lower in Figure 4c than in Figure 4d.

Figure 5 shows the structure of invariant manifolds governing the bifurcation at $\omega = 1.02$, very near the lowest frequency at which there is a nonzero probability of escape. It should be noted that unlike Figure 2, Figure 5 shows only parts of the invariant manifolds: even

within the region depicted in Figure 5, many parts of the invariant manifolds are not shown, so as to highlight the essential features. For example, only four disconnected pieces of the inset *in* $({}^1D)$ of the hilltop saddle ${}^1D$ are shown: one piece (two branches) approaching ${}^1D$ itself, plus three pieces of parabolic shape passing through points 1 and 2, 3 and 4, 5 and 6 respectively. Since the inset and outset of ${}^1D$ intersect, they form a homoclinic tangle, so infinitely many additional pieces of the inset *in* $({}^1D)$ must exist, including pieces which accumulate on the four pieces shown. Futhermore, only one branch of the outset of D^3 is shown, and although some homoclinic intersection points are clearly visible, the outset is folded so closely onto itself that it would not be possible to separate its layers without magnification. A more complete view of the global structure can be gleaned from Stewart (1988), Ueda et al. (1988), or Guckenheimer and Holmes (1983). The apparently fractal basin structure in Figure 4c attests to the existence of portions of *in* $({}^1D)$ not shown in Figure 5. Although *in* $({}^1D)$ is not a smooth basin boundary in the sense of Grebogi et al. (1987), any small neighborhood of any part of *in* $({}^1D)$ will surely contain points in the basins of both ${}^1S$ and ${}^1S'$; this fact leads us to a sufficient condition for the outcome of a chaotic blue sky catastrophe to be indeterminate.

The possibility of two outcomes exists because there is a transverse heteroclinic intersection between the outset of the destroyer D^3 and the inset of the hilltop saddle ${}^1D$, indicated in Figure 5 by the heteroclinic points numbered 1 through 6. Since the inset of ${}^1D$ is the basin boundary shared by ${}^1S$ and ${}^1S'$, this heteroclinic intersection implies that a transient leaving the former chaotic attractor following

the outset of D^3 may lie on either side of the knife edge, the inset of ${}^1D$. The short segment of solid arc in Figure 3 passing through point R indicates the (ω, A) locus of a heteroclinic tangency *in* $({}^1D) \cap$ *out* (D^3), where points 1 and 2 would coincide. For parameter values (ω, A) above this short segment of solid arc through R, there is persistent heteroclinic intersection, and thus surely the outset *out* (D^3) includes points in the basins of both ${}^1S$ and ${}^1S'$. On the other hand, for parameter values (ω, A) below this segment of arc, the heteroclinic intersection shown in Figure 5 will be absent; but there may be a heteroclinic intersection of *out* (D^3) with a portion of *in* $({}^1D)$ not shown in Figure 5. Thus for the outcome to be indeterminate, it is sufficient but not necessary to cross the bifurcation arc G to the right of point R. In fact, the outcome does become determinate just a small distance to the left of point R.

As noted above, transverse homoclinic intersection of the inset and outset of the hilltop saddle guarantees that the basin boundary between ${}^1S$ and ${}^1S'$ is tangled. Indeed, the inset of ${}^1D$ cannot heteroclinically intersect the outset of D^3 without homoclinically intersecting the outset of ${}^1D$, so in this regime an indeterminate blue sky catastrophe is always governed by a fractal basin boundary. This implies a qualitatively greater degree of uncertainty than in our first example, which was governed by a heteroclinic structure but no homoclinic structure. For instance, there is here a thick Cantor-like set of disturbance sizes for which the outcome will be infinitely sensitive to the disturbance size. In our first example, the sensitivity was infinite only for a denumerable set of disturbance sizes, related to the denumerable sequence of heteroclinic points.

The fractal basin structure in the present example means that in principle the probabilities of the two outcomes will be much harder to estimate from knowledge of a few heteroclinic points. By comparing Figure 4d and Figure 5, it is clear that not all points on the outset of D^3 between heteroclinic points 1 and 2, say, will settle to ${}^1S'$, nor will all points between 2 and 3 end up on ${}^1S$. In addition to the spacing of heteroclinic points such as 1 through 6, one would also need to know the proportions to which the basins are mixed in the fractal structure created by the homoclinic tangling of ${}^1D$. Near ${}^1D$ the local linear theory would be applied to determine the basin proportions locally, but we cannot in general expect those local proportions near ${}^1D$ to be correct near D^3. So the spacing of heteroclinic points 1 through 6 gives only a crude estimate of outcome probabilities, and it would be quite difficult to refine this crude estimate.

This difficulty in estimating the outcome probabilities is due to the tangling of the outcome basins, and is unrelated to the fact that the disappearing attractor is chaotic. Thus the same considerations would apply to the indeterminate saddle-node bifurcation with fractal outcome basins discovered by Thompson and Soliman (1990). We note that a similar bifurcation occurs in equation (2) crossing the fold arc F between Q and S, where S is defined by a heteroclinic tangency of the inset of ${}^1D$ with the outset of ${}^2D$. In Figure 3, the locus of this tangency in (ω, A) is indicated by a short segment of arc just below and nearly parallel to the arc defining point R. Indeed Figure 5 shows ${}^2D$ lying very close to the outset of D^3, and their outsets are almost parallel in the region near points 1 through 6.

A rough estimate of the probability of escape can be derived as

follows. As in the previous example, we have chosen the heteroclinic points 1 through 6 for convenience: they correspond to the coarsest, most readily apparent structure in Figure 4c. However, for accurate estimation of probabilities, pre-images much closer to D^3 would be preferred. The coordinates and distances are given in Table 2. For instance, under the lowest order assumption that all points between 1 and 2 lead to escape while all points between 2 and 3 lead to recapture (i.e. ignoring the fractal basin structure), roughly 9% escape outcomes are estimated. (Since the destroyer has period 3, we should consider a fundamental neighborhood of its outset between a heteroclinic point H and its image H^* under three iterations of the Poincaré map; the point numbered 3 is the image of point 1 under one iteration.)

A numerical experiment was performed starting from 200 orbits settled on the chaotic attractor at $\omega = 1.02$, $A = 0.1971$ for more that 100 iterations; then increasing A to 0.1972 and iterating until each of the 200 orbits settled to either ${}^1S$ or ${}^1S'$. The results were 25 escapes to ${}^1S'$ and 175 recaptures by ${}^1S$.

To summarize, we have presented two examples of bifurcations in which an attractor undergoes a complete loss of stability and the system jumps to one of two other coexisting attractors. In both cases the attractor ultimately chosen depends very sensitively on the precise details of how the bifurcation is realized, for example the precise size of a step increment in the bifurcation parameter. Although both examples are strictly speaking deterministic, in practice we may say that the outcome of the bifurcation is indeterminate. The outcomes are governed by the structure of invariant manifolds and well-defined probabilities can be assigned. In one case, where only a relatively sim-

ple heteroclinic structure occurs, the probabilities can be estimated from knowledge of just a few heteroclinic points. In the other case, both heteroclinic and homoclinic structures occur, the outcome basins have a more complicated, fractal boundary, and estimating probabilities is substantially more difficult.

We are grateful to Ralph Abraham, Michael Thompson, and Yannis Kevrekidis for stimulating discussions. A numerical survey of the twin-well Duffing equation by Caryn Sarfati gave us the basis for Figure 3; her work was supported by the Science and Engineering Research Semester Program of the U.S. Department of Energy. H.B.S. acknowledges with gratitude the support of the Applied Mathematical Sciences program of the U.S. Department of Energy. Y.U. would like to acknowledge use of the facilities of the Computer Center of the National Institute for Fusion Science at Nagoya.

Table 1. Distances between heteroclinic points in Figure 2.

Point	x	y	distance $(n, n+1)$
1	-.945	.509	.032
2	-.957	.479	.284
3	-1.010	.200	.048
4	-1.011	.152	.385
5	-.936	-.226	.054
6	-.911	-.274	.405
7	-.576	-.501	.067
8	-.509	-.507	

Table 2. Distances between heteroclinic points in Figure 5.

Point	x	y	distance $(n, n+1)$
1	.230	-.017	.016
2	.241	-.006	.160
3	.365	.095	.014
4	.376	.103	.062
5	.426	.139	.006
6	.431	.142	

List of Figures

References

Abraham, R.H. 1985 Chaostrophes, intermittency and noise. In *Chaos, Fractals, and Dynamics* (ed. P. Fischer and W.R. Smith), pp. 3–22. New York: Marcel Dekker.

Abraham, R.H. and Shaw, C.D. 1987 Dynamics: a visual introduction. In *Self-Organizing Systems* (ed. F.E. Yates), pp. 543–597. New York: Plenum.

Grebogi, C., Ott, E., and Yorke, J.A. 1983 Crises, sudden changes in chaotic attractors, and transient chaos.*Physica* D **7**, 181–200.

Grebogi, C., Ott, E., and Yorke, J.A. 1987 Basin boundary metamorphoses: changes in accessible boundary orbits. *Physica* D **24**, 243–262.

Guckenheimer, J., and Holmes, P. 1983 *Nonlinear oscillations, dynamical systems, and bifurcations of vector fields*. New York: Springer-Verlag.

Rössler, O.E. 1976 An equation for continuous chaos. *Phys. Lett.* **57A**, 397–398.

Stewart, H.B. 1988 A chaotic saddle catastrophe in forced oscillators. In *Dynamical Systems Approaches to Nonlinear Problems in Systems and Circuits* (eds. F. Salam and M. Levi), pp. 138–149, Philadelphia: SIAM.

Takens, F. 1974 Forced oscillations and bifurcations. *Comm. Math. Inst. Univ. Utrecht* **3**.

Thompson, J.M.T. 1987. Chaotic phenomena triggering the escape from a potential well. *Proc. R. Soc. Lond.* A**421**, 195–225.

Thompson, J.M.T. and Soliman, M.S. 1990 Indeterminate jumps to resonance from a tangled saddle-node bifurcation. Submitted to Proc. R. Soc. Lond. A.

Ueda, Y. 1980 Steady motions exhibited by Duffing's equation: a picture book of regular and chaotic motions. In *New Approaches to Nonlinear Problems in Dynamics* (ed. P.J. Holmes), pp. 311–322, Philadelphia: SIAM.

Ueda, Y., Nakajima, H. Hikihara, T., and Stewart, H.B. 1988 Forced twin-well potential Duffing's oscillator. In *Dynamical Systems Approaches to Nonlinear Problems in Systems and Circuits* (eds. F. Salam and M. Levi) pp. 128–137, Philadelphia: SIAM.

Zeeman, E.C. 1982 Bifurcation and catastrophe theory. In *Papers in Algebra, Analysis and Statistics* (ed. R. Lidl), pp. 207–272. Providence, R.I.: Amer. Math. Soc.

Fig. 1

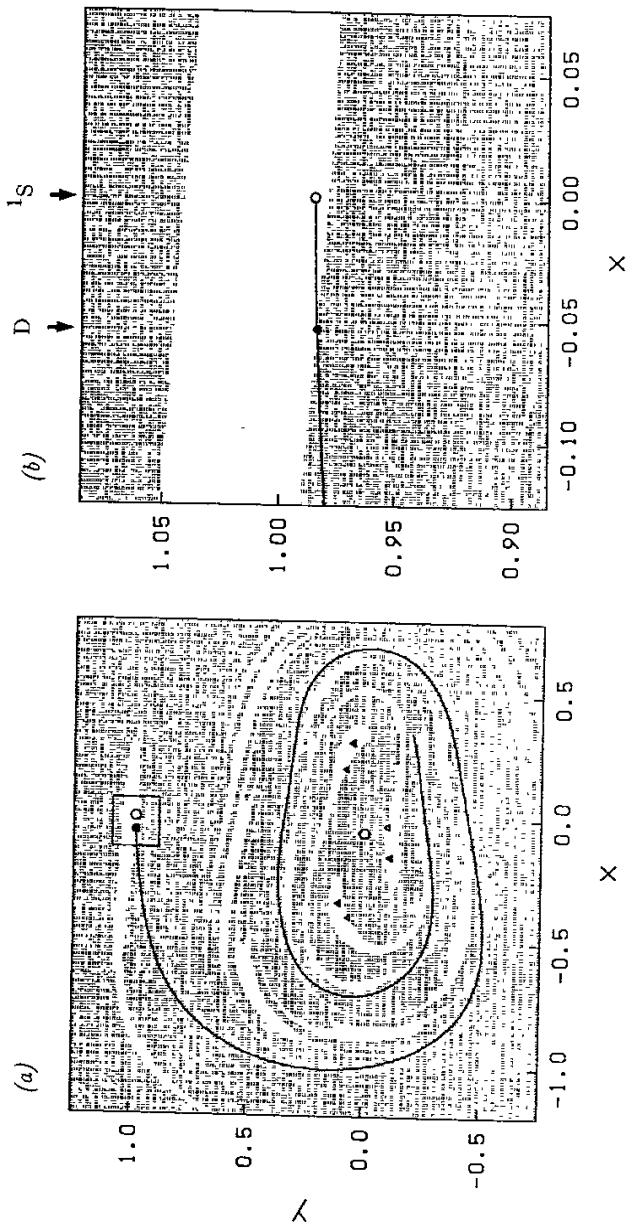

Fig. 2

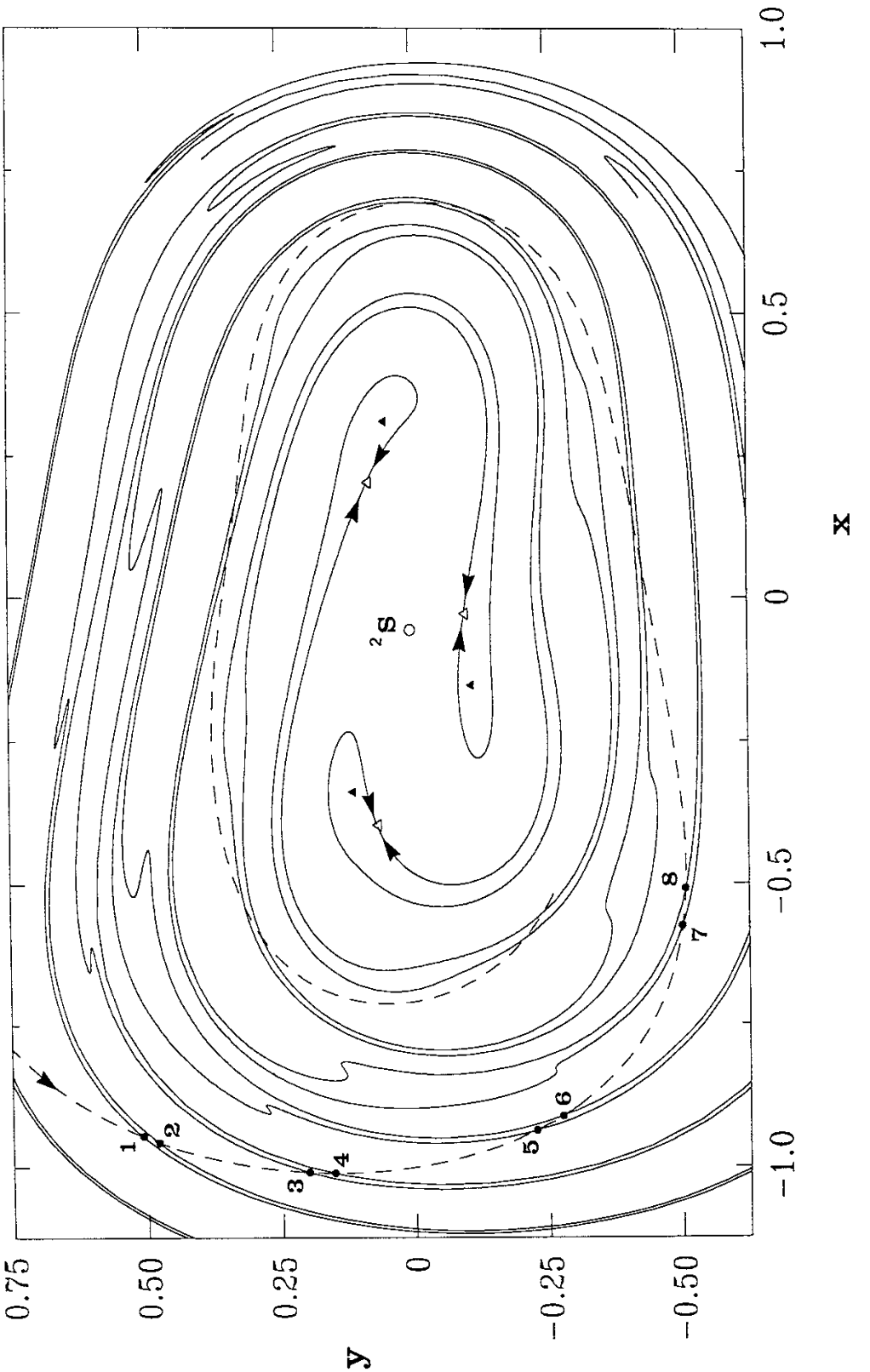

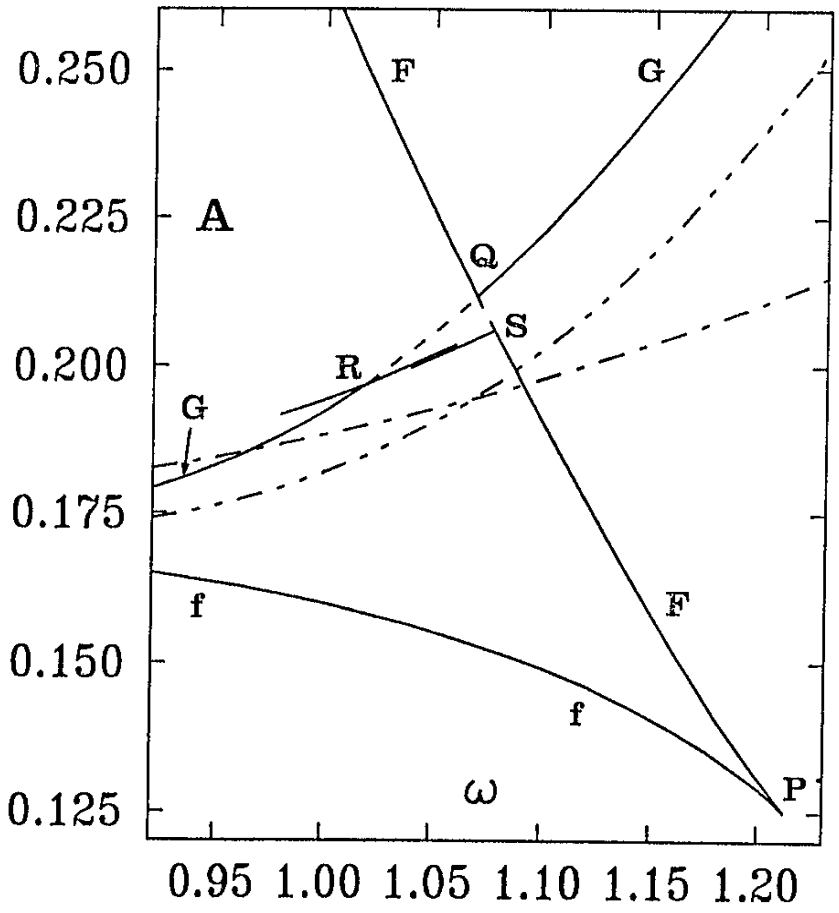
0.250
0.225
0.200
0.175
0.150
0.125
A
F
G
Q
S
R
G
f
F
f
P
ω
0.95 1.00 1.05 1.10 1.15 1.20

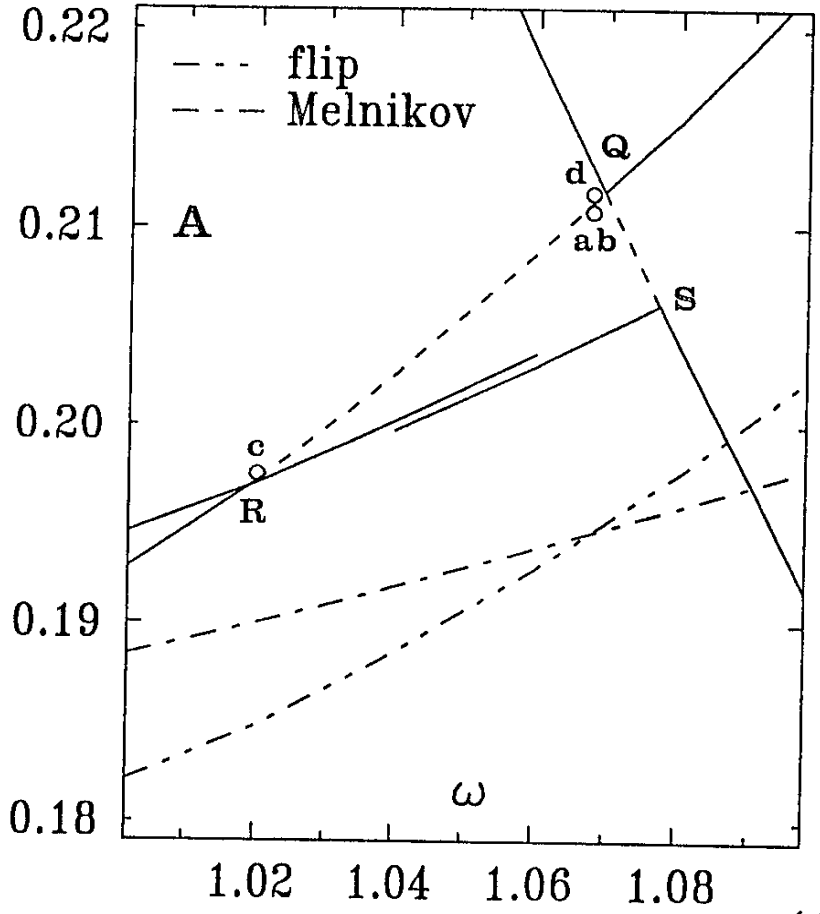
0.22
0.21
0.20
0.19
0.18
flip
Melnikov
A
Q
d
a b
S
c
R
ω
1.02 1.04 1.06 1.08

Fig. 3

Fig. 4

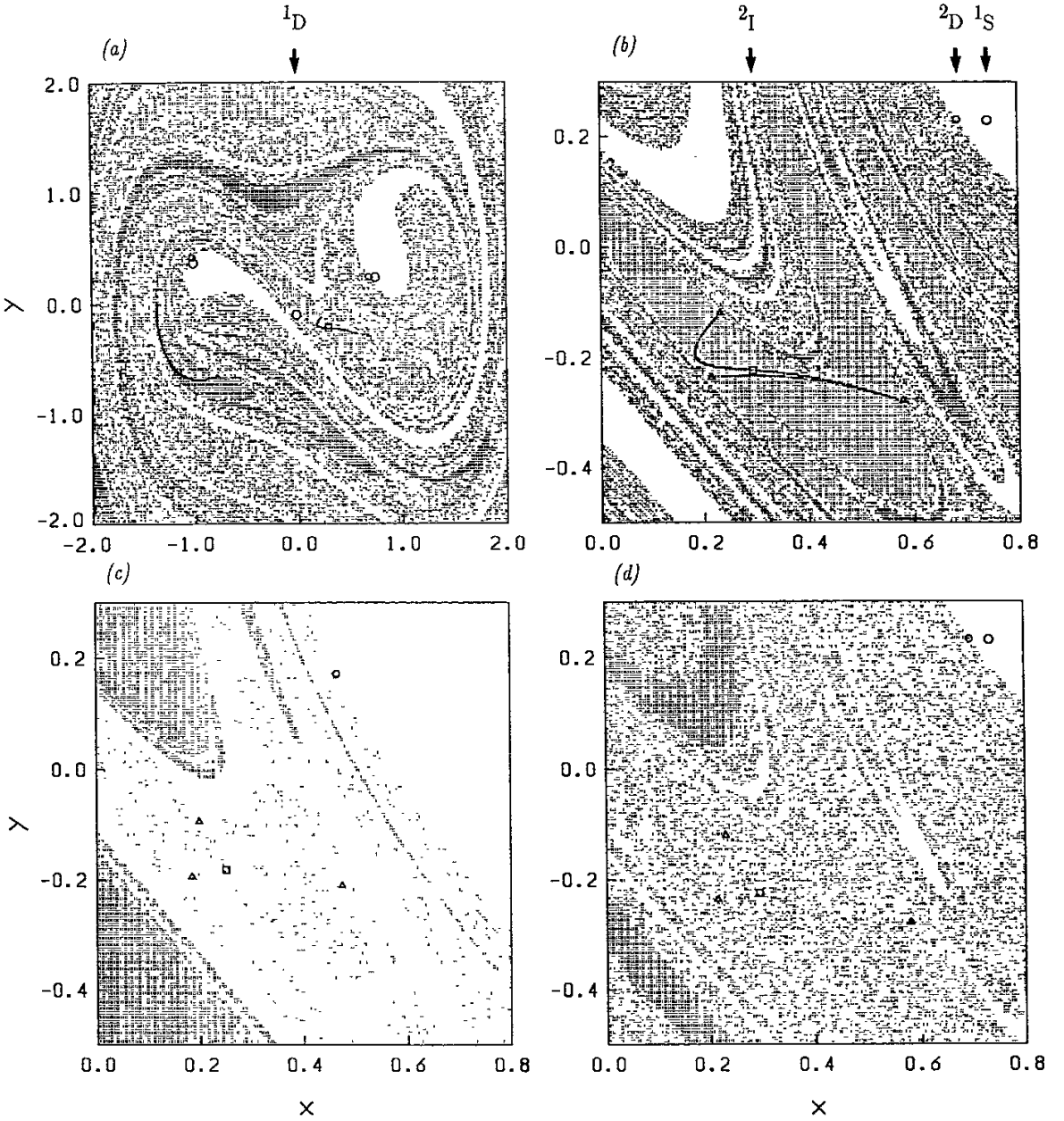

Fig. 5